Rock Mechanics and Rock Engineering (2019) 52:2585–2603
https://doi.org/10.1007/s00603-018-1711-y

ORIGINAL PAPER

Damage Analysis of High-Temperature Rocks Subjected to LN_2 Thermal Shock

Xiaoguang Wu[1] · Zhongwei Huang[1] · Shikun Zhang[1] · Zhen Cheng[1] · Ran Li[1] · Hengyu Song[1] · Haitao Wen[1] · Pengpeng Huang[1]

Received: 25 February 2018 / Accepted: 5 December 2018 / Published online: 7 January 2019

Abstract

Liquid nitrogen (LN_2) fracturing is a technology that can dramatically enhance the stimulation performances of high-temperature reservoirs, such as hot dry rock geothermal and deep/ultra-deep hydrocarbon reservoirs. The aim of the present study was to investigate the damage characteristics of high-temperature rocks subjected to LN_2 thermal shock, which is a critical concern in the engineering application of LN_2 fracturing. In our work, the rocks (granite, shale and sandstone) were slowly heated to different temperatures (25 °C, 150 °C and 260 °C) and maintained at the target temperatures for 10 h, followed by LN_2 quenching. After thermal treatments, we tested the physical and mechanical properties of the rocks to evaluate their damages. Additionally, sensitivities of the three rocks to thermal shock were also compared and analyzed. According to our experiments, LN_2 thermal shock can enhance the permeability of the rocks and deteriorate their mechanical properties significantly. Increasing rock temperature helps strengthen the effect of LN_2 thermal shock, leading to more severe damage. Inter-granular cracking is the primary contribution to the rock damage in the LN_2 cooling process. Compared with granite and shale, sandstone is less sensitive to LN_2 thermal shock. The lower sensitivity of sandstone to thermal shock is mainly attributed to its larger pore spaces and weaker heterogeneity of mineral thermal expansion. The present paper can provide some guidance for the engineering application of LN_2 fracturing technology.

Keywords Rock damage · Thermal shock · Rapid cooling · Liquid nitrogen · Waterless fracturing

List of Symbols

V_p	P-wave velocity (m/s)
P_c	Confining pressure, MPa
P_o	Pore pressure (MPa)
ΔP_o	Upstream pressure increment (KPa)
P_d	Downstream pressure (MPa)
t	Time (min)
V_u	Upstream volume (mL)
V_d	Downstream volume (mL)
L	Length of rock sample (m)
A	Cross area of rock sample (m^2)
μ	Dynamic viscosity of nitrogen (1.8×10^{-5} Pa s)
K_1	Permeability after heating and LN_2 cooling, $\times10^{-3}\mu m^2$
K_a	Permeability after heating and air cooling, $\times10^{-3}\mu m^2$
Δ_K	Thermal shock induced permeability growth rate, %
K	Permeability, $\times10^{-3}\mu m^2$
E	Young's modulus, GPa
σ_{ca}	Compression strength after heating and air cooling, MPa
σ_{cl}	Compression strength after heating and LN_2 cooling, MPa
$\Delta\sigma_c$	Thermal shock-induced strength reduction rate, %
σ	Standard deviation
φ	Content of quartz, %
VC	Variation coefficient
T	Temperature, ℃
β	Average thermal expansion coefficient, /℃
β_q	Thermal expansion coefficient of quartz, /℃
β_{nq}	Average thermal expansion coefficient of non-quartz minerals, /℃

✉ Zhongwei Huang
huangzw@cup.edu.cn

[1] State Key Laboratory of Petroleum Resources and Prospecting, China University of Petroleum-Beijing, Beijing 102249, China

1 Introduction

High-temperature reservoirs, such as hot dry rock (HDR), geothermal reservoirs and deep/ultra-deep hydrocarbon reservoirs, have recently attracted attention (Breede et al. 2013; Ghassemi 2012; Hu et al. 2018b; Shi et al. 2018; Wenrui et al. 2013). In these reservoirs, stimulation is usually needed to create pathways with sufficient permeability. Liquid nitrogen (LN_2) fracturing, as one of the waterless stimulation technologies, has the prospect for broad application in such reservoirs (Alqatahni et al. 2016; Cha et al. 2014). Compared to conventional water fracturing, LN_2 fracturing is able to address issues such as environmental contamination, reservoir damage and large water consumption (Cai et al. 2016; Wang et al. 2016a). Furthermore, LN_2 is a cryogenic fluid with the boiling temperature of − 196.8 °C under atmospheric pressure (Jacobsen et al. 1986). Cryogenic LN_2 can significantly deteriorate rocks and enhance the permeability of formations. Therefore, damage of high-temperature rocks subjected to LN_2 cooling is a great concern in engineering applications of LN_2 fracturing.

Sudden temperature changes, also referred to as thermal shock, can generate extremely high thermal stress due to the differential contraction of exterior parts and interior parts of rocks (Hu et al. 2018a). During cooling, the exterior region of rock is in tension, and the maximum tensile stress appears on the cooling surface. The magnitude of the thermal stress highly depends on the cooling rate (Kim et al. 2014; Kim and Kemeny 2009). Higher cooling rates help generate steeper temperature gradients and greater thermal stresses in the solid (Zhang et al. 2017b). Boiling heat transfer of LN_2, as an efficient heat transfer enhancement method, has a very high cooling rate. Hence, LN_2 cooling can induce extremely high tensile stresses in rocks and promote the initiation and propagation of micro-cracks. In addition to the temperature gradient, the mismatch in thermo-physical properties between different minerals also contributes a lot to the rock damage induced by thermal shock (Johnson 1978). Rock is a mixture composed of diverse minerals. The elastic modulus and the thermal expansion coefficient are greatly different for various minerals. Compared with other minerals, quartz has a significantly higher thermal expansion coefficient (Igarashi et al. 2015). During rapid cooling, the difference in the thermal expansion coefficient between quartz and other minerals can lead to the failure of cementation structures, creating many inter-granular cracks in the rock. Even for the same mineral, the thermal expansion coefficients in different crystallographic directions are also significantly different. For example, the thermal expansion coefficient of quartz perpendicular to the *c* axis (14×10^{-6}/°C) is approximately 2 times higher than that parallel to the *c* axis (7.7×10^{-6}/°C) (Johnson and Parsons 1944). Due to the differential deformations of such minerals in different crystallographic directions, rapid cooling will generate many intra-granular cracks, which dramatically intensify the damage of quartz rich rocks.

Many priors have investigated the effect of thermal shock on the physical and mechanical behaviors of rocks (Kumari et al. 2017a, b; Shao et al. 2014; Tarragó et al. 2016; Zhang et al. 2018; Zhou et al. 2016). The thermal shock in most of their experiments is implemented by water quenching. They found that the thermal shock can extend the intrinsic cracks in rocks and reduce the rock strength significantly and thus has a positive influence on the hydraulic fracturing performance of HDR reservoirs. According to the experimental results reported by Zhou et al. (2016), the cracks induced by thermal shock near the wellbore facilitate the initiation and propagation of hydraulic fractures, improving the permeability of the formation dramatically. Moreover, the cyclic thermal shock treatment has a more significant impact on the physical and mechanical properties of rocks. Previous studies indicate that the mechanical deterioration and permeability improvement of rocks become more significant with increasing cycles of thermal shock treatment (Wang et al. 2016b, 2017; Yavuz et al. 2006).

Compared with water cooling, LN_2 quenching is a more violent heat transfer process. Wu et al. (2018) and Cai et al. (2014, 2015) investigated the effect of thermal shock induced by LN_2 quenching experimentally. The scanning electron microscope (SEM) and nuclear magnetic resonance (NMR) were adopted by them to reveal the micro-mechanisms of rock failure. According to their experimental results, LN_2 thermal shock deteriorates the mechanical properties of rocks significantly. The NMR and SEM results indicate that the mechanical changes of rocks subjected to LN_2 quenching are mainly attributed to the expansion of micro-fissures and the growth of pore scale. Similar to cyclic water quenching, cyclic LN_2 quenching can also intensify the damage of rocks. Qin et al. (2017a, b, 2018a, b) conducted a series of experiments to investigate the heat transfer, changes in petrophysical properties and the fracture propagation of coal samples subjected to cyclic LN_2 injection. They found that the coal after a single LN_2 thermal shock treatment could be damaged, but the damage was just limited to the area adjacent to the injection tube. However, the cyclic treatment of LN_2 thermal shock increased damage area significantly and formed a propagated fracture network in the rock specimens. Due to the unique characteristics of the cryogenic LN_2, some priors have proposed to apply LN_2 in rock breaking and well drilling (Cai et al. 2016; Zhang et al. 2017a, 2018). Wu et al. (2018a) conducted rock-breaking experiments with the high-velocity LN_2 jet.

The results indicate that the LN_2 thermal shock effect can greatly improve the rock-breaking efficiency by creating cracks in rock and simultaneously reduce the specific energy of rock failure.

According to the literature review, current researches are mainly focused on the responses of room-temperature rocks to LN_2 thermal shock, while the thermal shock effect on high-temperature rocks and the damage difference between different rocks are still unclear. In the present paper, we aimed to study the effect of LN_2 thermal shock on three different high-temperature rocks (sandstone, shale and granite). Permeability tests and compression strength tests under different confining pressures were conducted to determine the physical and mechanical behaviors of rocks subjected to LN_2 thermal shock. Additionally, potential causes of the thermal sensitivity discrepancy among the three rocks were discussed based on scanning electron microscopy (SEM) and X-ray diffraction (XRD) analyses. The present research is expected to provide a better understanding of the damage characteristics and mechanisms of high-temperature rocks subjected to LN_2 thermal shock.

2 Materials and Methods

2.1 Rock Specimen Preparation

Figure 1 shows the rock samples and test instruments used in our experiment. Three different rocks, i.e., granite, sandstone and shale, were used and compared. These rocks were cut into cylinders with dimensions of 50 mm in height and 25 mm in diameter. It should be noted that shale samples were cored in the direction vertical to bedding planes in this work. For each rock species, four intact samples (samples without thermal treatment) were tested to obtain the average physical and mechanical properties. Detailed physical and mechanical properties of the intact samples are shown in Table 1. The granite is collected from Shandong province in China. The average density and permeability of the granite are 2618 kg/m^3, 0.0067×10^{-3} μm^2 (tested under the confining pressure of 2 MPa), respectively. It is mainly composed of quartz (28.3%), plagioclase (41.9%) and K-feldspar (15.7%). The sandstone used in the experiment is a medium-grain sandstone with a density of 2396 kg/m^3. It was collected from an oil field in eastern China, and the formation depth of

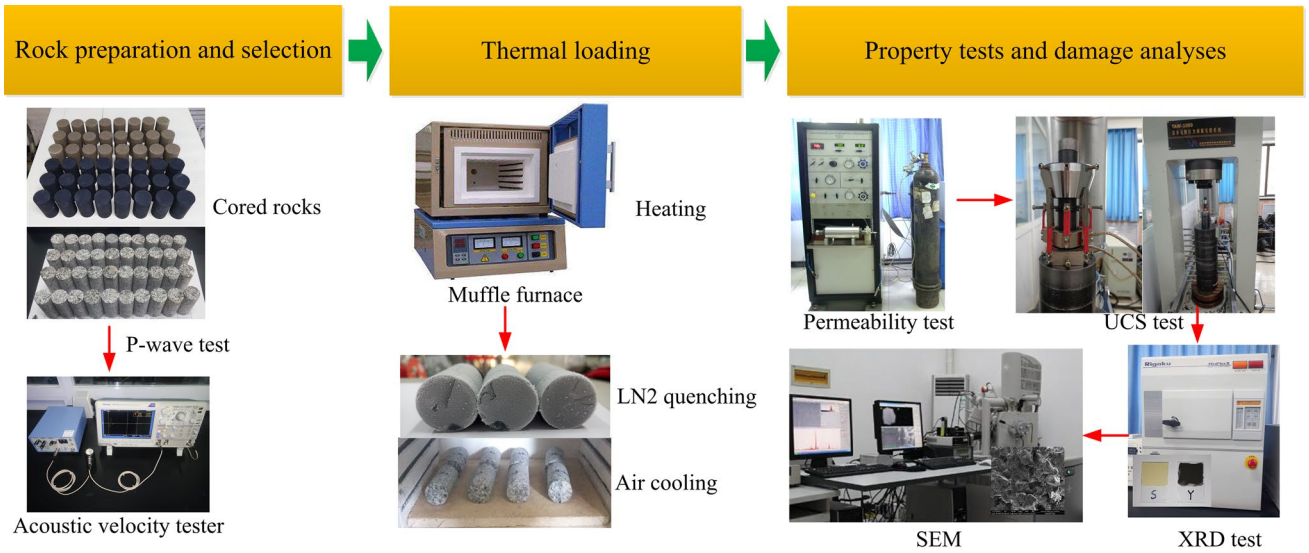

Fig. 1 Rock samples and experimental instruments

Table 1 Average physical and mechanical properties of the intact samples

Confining pressure	Permeability ($\times 10^{-3}$μm^2)		Compression strength (MPa)		Elastic modulus E (GPa)	
	2 MPa	40 MPa	0 MPa	40 MPa	0 MPa	40 MPa
Granite	0.006745	0.000874	147.8	548.3	33.8	39.6
Shale	0.000362	0.000035	186.6	293.6	9.5	31.6
Sandstone	0.145691	0.004062	65.3	210.9	27.8	12.9

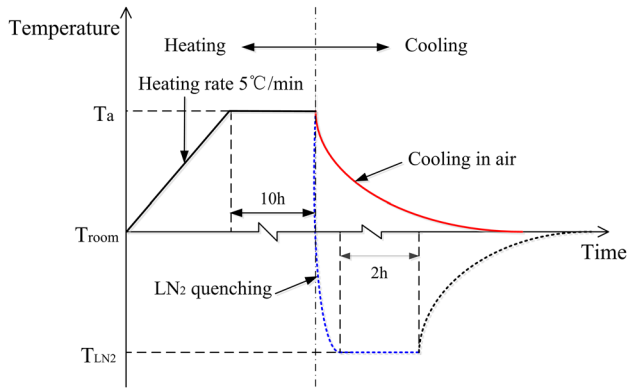

Fig. 2 Thermal loading schedule

Table 2 The scheme of the permeability test

Test	Confining pressure P_c (MPa)	Pore pressure P_o (MPa)	Net confining pressure $P_c - P_o$ (MPa)	Pressure increment ΔP_o (KPa)
Test I	9	7	2	70
Test II	70	30	40	70

this sandstone was approximately 2500 m. The average permeability is 0.1457×10^{-3} μm^2. The main composition minerals are quartz (56.9%) and plagioclase (19.1%). The shale was cored from Sichuan basin, China. Its strength is significantly higher than those of the other two rocks. Nevertheless, its permeability is the lowest among the three rocks, which is just 0.00036×10^{-3} μm^2. The density of the shale is 2520 kg/m^3. Unlike the other two rocks, clay mineral (20.6%) in shale is much richer in content.

We dried the rock samples in an air-drying oven before the experiment and then tested their longitude wave velocities (P-wave velocity, V_p). To weaken the influence of rock heterogeneity, only the samples with similar V_p values were used in our experiments. The P-wave velocity test is a common non-destructive test that can be used to detect the intrinsic flaws in rocks. The physical and mechanical properties of samples with similar V_p values are usually at the same level. Thus, sample selection through the P-wave velocity test ensures the comparability of rocks in different groups.

2.2 Thermal Loading Schedule

The thermal loading schedule is shown in Fig. 2. We first heated the rocks to different target temperatures (25 °C, 150 °C and 260 °C) using a muffle furnace with a heating rate of 5 °C/min and then kept them at the final temperature for 10 h. Afterwards, two cooling methods, (1) LN_2 quenching and (2) cooling naturally in air, were implemented to cool down the high-temperature rocks. Air cooling, as a very slow cooling way, has very weak thermal shock effect and cannot induce significant deterioration in rock properties (Kumari et al. 2017b). Thereby, we can distinguish the effect of LN_2 thermal shock on rock damage by comparing the physical and mechanical properties after LN_2 quenching with those after cooling in air.

2.3 Instruments and Test Methods

2.3.1 Permeability Test

Considering that rocks such as shale have ultra-low permeability, we used the transient-pulse permeability test method

Table 3 Permeability of rock samples after different thermal loadings

Rock species	Cooling way	Permeability under net confining pressure of 2 MPa ($\times 10^{-3}$μm^2)			Permeability under net confining pressure of 40 MPa ($\times 10^{-3}$μm^2)		
		25 °C	150 °C	260 °C	25 °C	150 °C	260 °C
Granite	LN_2 cooling	0.011486	0.016310	0.028656	0.000904	0.001155	0.002404
		0.012440	0.013278	0.028343	0.000957	0.001121	0.002080
	Air cooling	0.006873	0.007759	0.010929	0.000887	0.000868	0.001141
		0.007494	0.007879	0.010478	0.000845	0.000906	0.001206
Sandstone	LN_2 cooling	0.138682	0.160588	0.191864	0.004245	0.004106	0.004791
		0.152959	0.150285	0.150012	0.004197	0.004019	0.005001
	Air cooling	0.168776	0.161809	0.166678	0.004252	0.004379	0.004612
		0.123562	0.151561	0.162555	0.004224	0.004110	0.005037
Shale	LN_2 cooling	0.000591	0.000728	0.001986	0.000040	0.000051	0.000156
		0.000423	0.000681	0.001970	0.000041	0.000070	0.000144
	Air cooling	0.000341	0.000536	0.001154	0.000038	0.000045	0.000106
		0.000372	0.000434	0.001055	0.000041	0.000056	0.000078

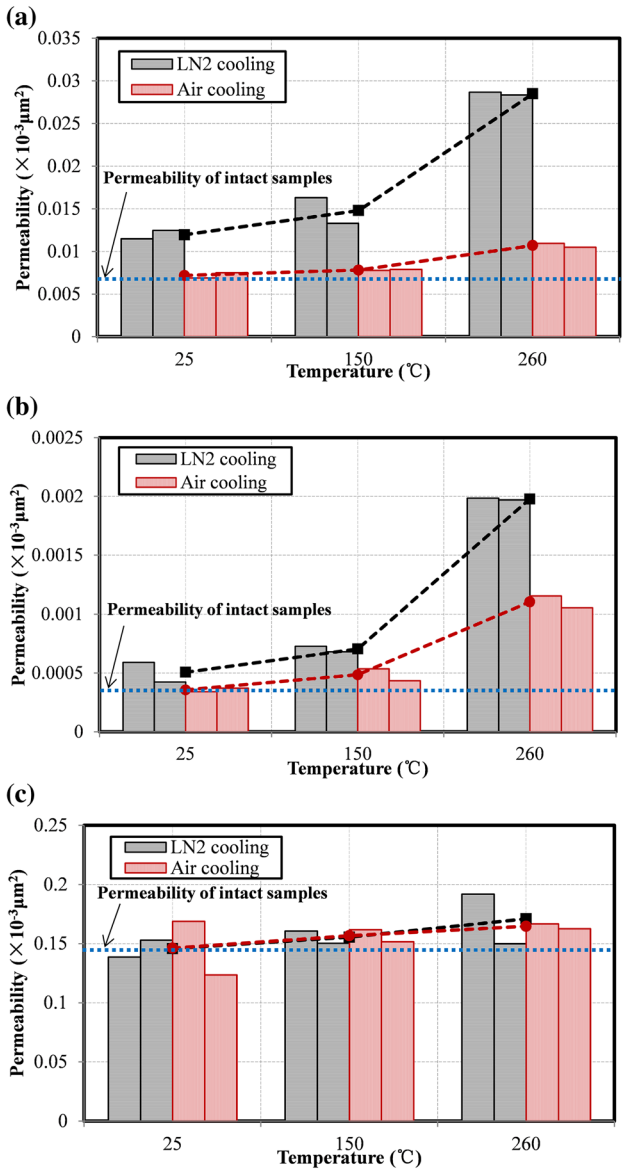

Fig. 3 Variations in permeability for **a** granite, **b** shale and **c** sandstone under the net confining pressure of 2 MPa

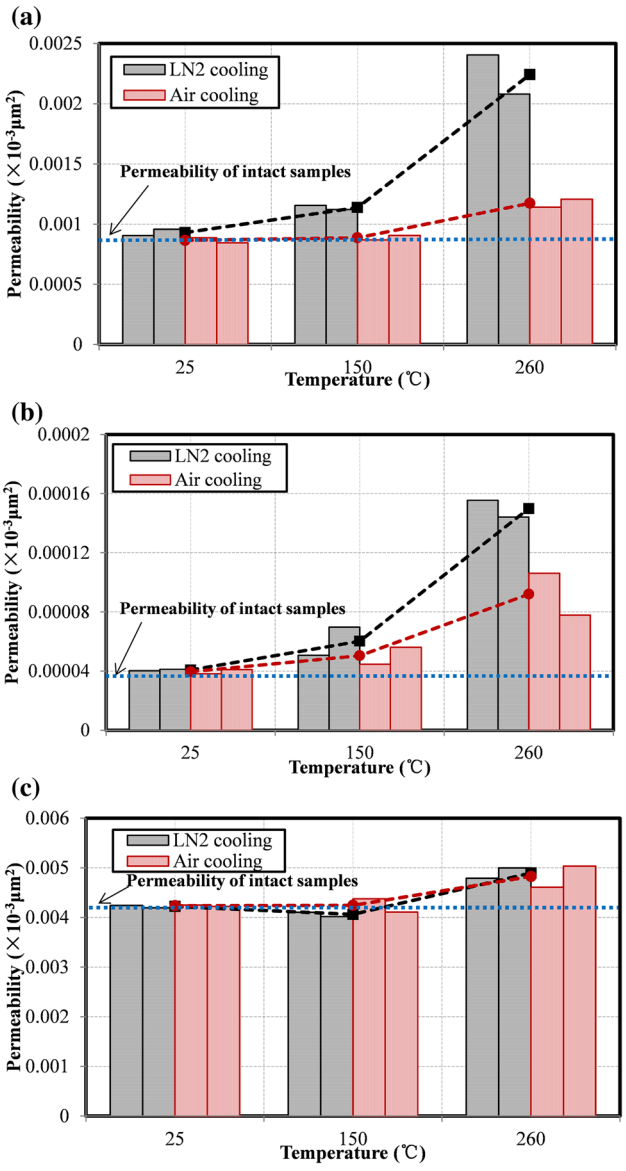

Fig. 4 Variations in permeability for **a** granite, **b** shale and **c** sandstone under the net confining pressure of 40 MPa

to guarantee the measurement accuracy. The test procedures of this method are summarized as follows:

1. Preheat the test device for 30 min.
2. Check the seal of the device, and place the sample into the device.
3. Load confining pressure P_c and pore pressure P_o with nitrogen.
4. Increase the upstream pressure by ΔP_o (70 KPa) to generate a pressure pulse.
5. Record the pressure attenuation data, and calculate the permeability.
6. The permeability K is calculated by the following equations (Yang et al. 2017):

$$K = -\frac{\mu L}{At}\frac{V_u V_d}{V_u + V_d}n \tag{2}$$

$$n = \ln\left(1 - \frac{P_d(t) - P_o}{\Delta P_o}\frac{V_u + V_d}{V_u}\right). \tag{3}$$

In the present paper, we performed the permeability tests under two different confining pressures, as shown in Table 2. The net confining pressures in test I and test II

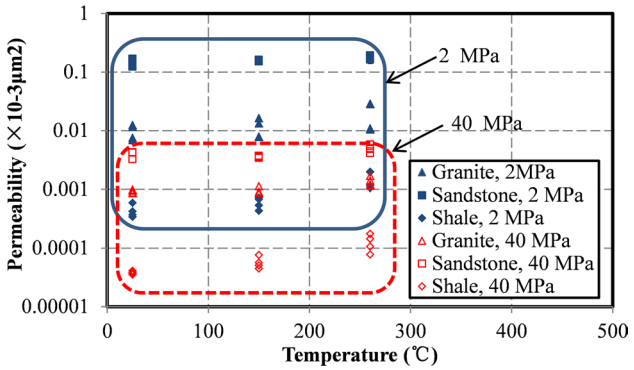

Fig. 5 The effect of confining pressure on the test results of permeability

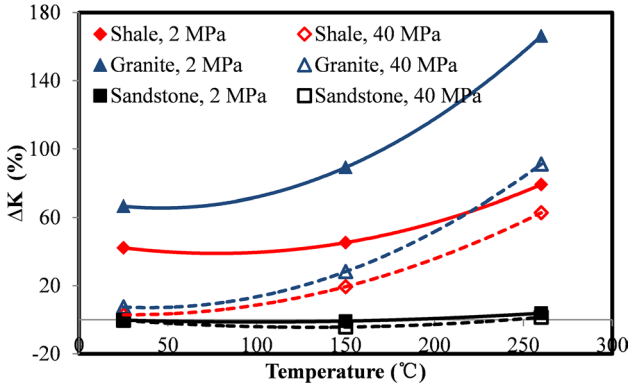

Fig. 6 Permeability change rate of the three rocks induced by LN_2 thermal shock

are 2 and 40 MPa, respectively. By comparing permeability results under different confining conditions, the effect of the confining pressures on the permeability can be determined. Considering that the depth of most high-temperature reservoirs (like HDR) usually ranges from 2000 m to 4000 m, the confining pressure used in test II was set to 70 MPa, which is at the same level as the in-situ stress at the average depth of 3000 m.

2.3.2 V_p Test and Mechanical Test

In our experiment, only samples with similar P-wave velocities were used. The P-wave velocity was measured using an ultrasonic pulse test device. During the measurement, the end surfaces of the rock samples were coated with Vaseline to ensure the effective connection of samples and transducers. We measured each rock sample three times. The changes in mechanical behaviors of rocks subjected to LN_2 thermal shock was determined by the uniaxial compressive strength (UCS) test and the triaxial compressive strength test. We conducted the mechanical tests using a TAW-1000 electro-hydraulic servo-controlled testing machine, which had a loading capacity of 1000 kN. Tests were displacement controlled and carried out at a constant rate of 0.05 mm/min. Axial and lateral displacements were recorded by displacement meters, whose full scale and accuracy were 100 mm and 0.5%, respectively.

2.3.3 XRD and SEM

To reveal the damage mechanisms of rocks subjected to LN_2 thermal shock, XRD and SEM analyses were performed on the treated rock samples. We tested the mineral composition of different rocks using a Rigatu MiniFlexII X-ray diffractometer. The mineral composition was obtained by analyzing the position (2θ) and intensity in the XRD spectra. Microstructures of rocks were observed using a FEI Quanta 200F scanning electron microscope. The maximum magnification of the SEM instrument was ×200,000, which was sufficient to determine the distribution of mineral grains and the micro-fissures induced by thermal shock in this work.

3 Results

3.1 Permeability

The permeability is an important parameter for porous materials such as rocks. It is commonly used to evaluate the capacity of rocks to allow fluid to flow through the pore space. We tested the permeability of the three rocks after thermal loading. The test results under two different confining conditions are shown in Table 3.

The permeability results tested under the net confining pressures of 2 and 40 MPa are plotted in Figs. 3, 4, respectively. It is obvious that the permeability of rocks increases after heating and subsequent cooling treatment, and the increasing magnitude becomes more significant at higher target heating temperature. For granite and shale, LN_2 cooling performs better in improving permeability compared with air cooling. However, for the sandstone, LN_2 cooling and air cooling achieve equivalent performances in permeability enhancement. The difference in the physical response to LN_2 cooling for the three rocks is closely related with the mineral compositions and microstructures, which will be detailed in Sect. 4.

Figure 5 shows the comparison in permeability between two different confining conditions. It indicates that the sandstone has the highest permeability, followed by granite and shale. The confining pressure has a great influence on the results of rock permeability. As the net confining pressure increases from 2 to 40 MPa, the rock permeability reduces by more than 10 times. The reason for this phenomenon is that the increasing confining pressure closes many voids and

Table 4 Mechanical properties of the rock samples subjected to different thermal loadings

Rock species	Temperature (ºC)	Cooling ways	Unconfined test		Confining pressure 40 MPa	
			Strength (MPa)	Modulus (GPa)	Strength (MPa)	Modulus (GPa)
Granite	25	Air	132.7	33.35	534.7	40.36
			149.6	34.94	549.6	41.13
		LN_2	132.3	33.10	533.0	40.57
			146.8	34.50	551.7	40.37
	150	Air	152.6	36.23	539.8	42.27
			169.3	36.20	548.8	42.69
		LN_2	135.0	29.48	516.1	38.57
			126.0	32.73	526.0	38.13
	260	Air	160.5	35.92	557.8	43.04
			167.3	36.33	573.7	42.10
		LN_2	119.8	30.12	500.2	37.65
			113.0	32.66	498.3	38.70
Sandstone	25	Air	60.7	9.50	206.5	13.01
			58.8	9.43	193.3	13.13
		LN_2	75.7	11.28	222.2	13.01
			73.0	10.87	195.4	12.90
	150	Air	67.7	9.32	220.4	13.02
			66.2	9.81	205.4	12.93
		LN_2	71.7	10.57	225.3	12.32
			70.5	9.72	215.3	12.46
	260	Air	72.6	10.12	230.6	13.99
			75.5	10.72	204.7	14.35
		LN_2	65.5	9.00	203.4	11.22
			62.9	9.04	221.5	11.98
Shale	25	Air	178.3	28.47	300.6	31.65
			181.4	28.22	290.4	32.21
		LN_2	170.0	25.89	303.7	31.65
			187.1	28.96	294.4	32.59
	150	Air	200.4	29.27	299.4	32.62
			212.6	29.41	310.4	33.21
		LN_2	180.5	29.26	301.4	30.11
			185.4	29.74	290.7	29.57
	260	Air	234.8	30.57	315.3	33.52
			201.8	30.85	320.6	33.15
		LN_2	147.6	29.57	272.5	29.56
			167.0	28.96	281.2	29.02

channels in rocks and thereby makes the fluid harder to flow through the rocks.

In our experiment, the changes in rock permeability are the joint action of heating and cooling. Considering all rock samples suffer from the same heating treatment, the only difference between the two thermal loadings is the thermal shock effect in the cooling process. The thermal shock is very weak in the air cooling process due to the slow cooling rate. However, compared with air cooling, LN_2 cooling has noticeably higher heat transfer rate, which can induce faster temperature drop, leading to strong thermal shock effect. Therefore, we take the permeability after heating and air cooling as a benchmark in present work to analyze the effect of LN_2 thermal shock on rock permeability. We define the LN_2 thermal shock induced permeability growth rate Δ_K as follows:

$$\Delta_K = \frac{K_l - K_{\mathrm{a}}}{K_{\mathrm{a}}}. \tag{4}$$

The permeability growth rates of rocks versus heating temperature are plotted in Fig. 6. The positive Δ_K values

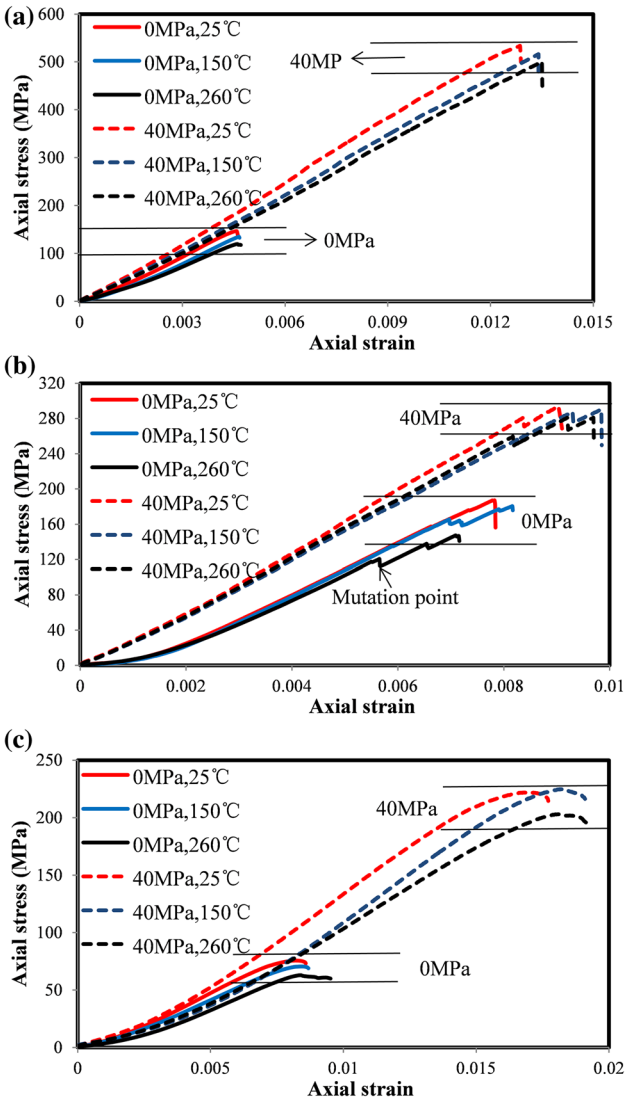

Fig. 7 Stress–strain curves of **a** granite, **b** shale and **c** sandstone subjected to heating and subsequent LN_2 quenching

indicate that LN_2 cooling is more superior in improving permeability than air cooling. The magnitude of Δ_K grows as rock temperature increases. It substantiates that the higher temperature contributes to aggravate the damage of rocks during LN_2 thermal shock. The permeability enhancement after LN_2 cooling treatment is mainly attributed to the thermal stress, which can create new microfissures and promote the propagation of pre-existed cracks in rocks. The thermal stress is positively correlated to the temperature change; thus rocks with higher temperatures suffer from greater thermal stress in the cooling process and are damaged more significantly. In addition, we also found in Fig. 6 that the confining pressure in the test also has a great impact on the permeability growth induced by LN_2 thermal shock. The values of Δ_K under the net confining pressure of 40 MPa are significantly lower than those under the net confining pressure of 2 MPa. However, it seems that the confining pressure does not influence the variation trend of Δ_K with temperatures. The Δ_K still shows a growing trend with increasing temperatures under the high confining pressure condition.

The sensitivity to LN_2 thermal shock is different for the three rocks. Under the net confining pressure of 2 MPa (as shown in Fig. 6), Δ_K of granite and shale increase by 66.5–166.26% and 42.22–79.09% (at the temperature range from 25 °C to 260 °C), respectively. Even under the higher net confining pressure (40 MPa), the LN_2 thermal shock induced permeability growth rate Δ_K for granite and shale can still reach 7.46–91.10% and 2.95–62.79%, respectively. However, it is not such a case for the sandstone used in our work. The Δ_K results of sandstone tested under two different confining pressures are almost same. The magnitudes of Δ_K only range from −4.29–3.87%, which are significantly lower than those of the other two rocks. Therefore, compared with granite and shale, the sandstone is more resistant to LN_2 thermal shock.

3.2 Mechanical Properties

Both uniaxial and triaxial compression tests were conducted to determine the thermal shock effect on the mechanical behaviors of different rocks. In the traixial compression tests, a confining pressure of 40 MPa is loaded on the samples. The failure stress and Young's modulus, as the most important two indicators of the mechanical deterioration, are summarized and shown in Table 4.

3.2.1 Axial Stress–Strain Curve

Figure 7a–c presents the stress–strain relationships of granite, shale and sandstone, respectively. Herein, only the curve of one sample in each group is plotted in the figures. It is obvious that the confining pressure in the tests has a great influence on the mechanical properties of rocks. Compared with the rocks without confining pressure (in the uniaxial tests), rocks tested under 40 MPa confining pressure have higher failure stress and failure strain (the strain at failure). Under high confining pressure conditions, the compaction stage becomes less noticeable in the compressive loading process. The stress–strain curves of shale differ from those of the other two rocks. Unlike the smooth curves of sandstone and granite, there are many stress mutation points on the shale curves. The stress mutation is usually considered as an indicator of local failures and mainly results from the interpenetration and nucleation of micro-cracks in the loading process (Cai et al. 2015). According to the test results, the shale samples at higher temperatures present more local failures in the loading process. This fact indicates that higher

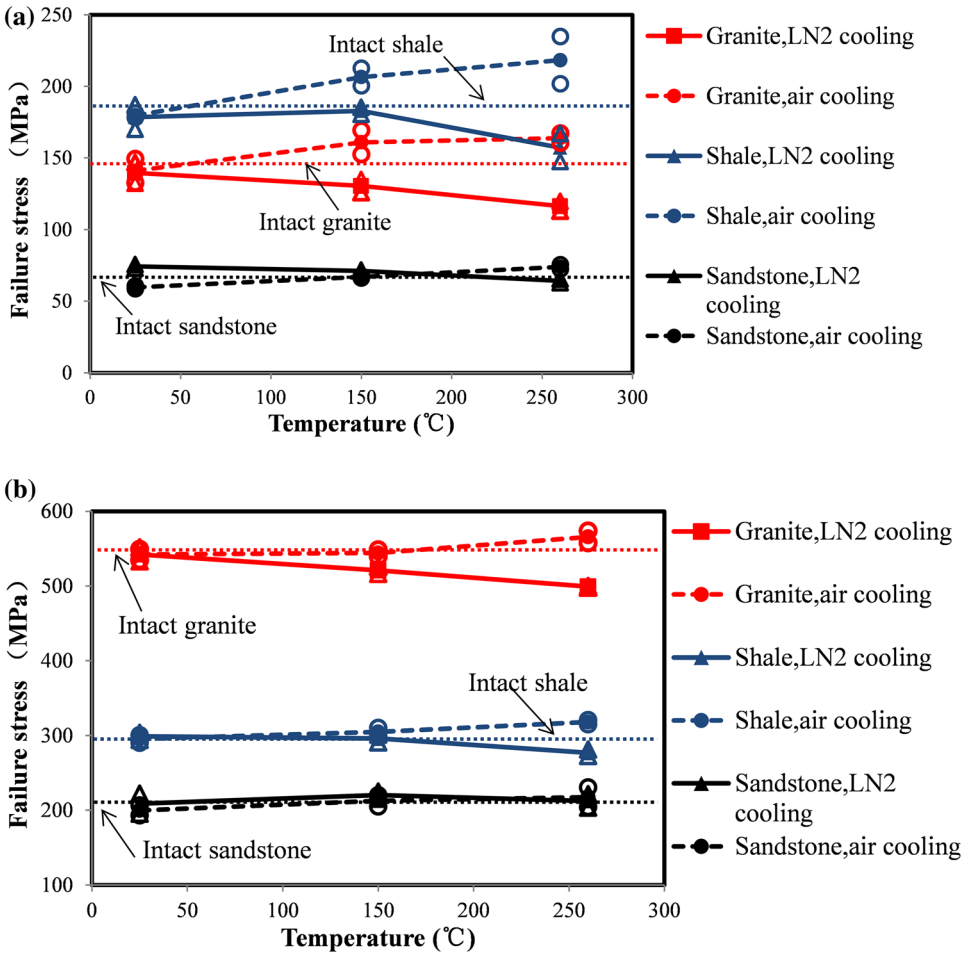

Fig. 8 Failure stresses of different rocks after thermal loading under **a** 0 MPa and **b** 40 MPa confining pressures

rock temperature can strengthen the LN_2 thermal shock effect and make the local damage of rocks subjected to LN_2 cooling treatment more significant.

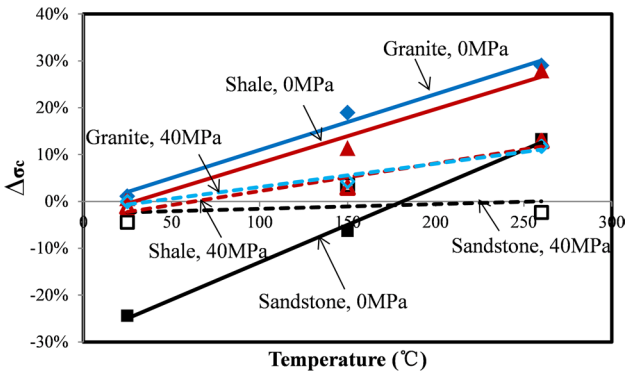

Fig. 9 Strength reduction rate $\Delta\sigma_c$ induced by LN_2 thermal shock for the three rocks

3.2.2 Failure stress

The failure stress in axial compression tests, also referred to as rock strength, is an important indicator of the mechanical deterioration of rocks. Figure 8a, b shows the results of failure stress tested under the confining pressures of 0 and 40 MPa, respectively. Under either confining condition, the failure stress of granite is the highest among the three rocks, followed by shale and sandstone. The sandstone is not as sensitive as the other two rocks to thermal treatments. The sandstones have very little change in failure stress after heating and cooling treatments. Even when the sandstone samples are heated to 260 °C, LN_2 thermal shock still cannot lead to significant strength reduction. Unlike the sandstone, the heating and subsequent cooling treatments have a significant influence on the failure stresses of granite and shale, and the effects of the two cooling ways are quite different. Failure stresses of shale and granite increase after heating and air cooling treatment, and the difference in the failure stress between the treated rocks and the intact rocks becomes more significant with increasing temperatures. In contrast to the heating and air cooling treatment, the heating

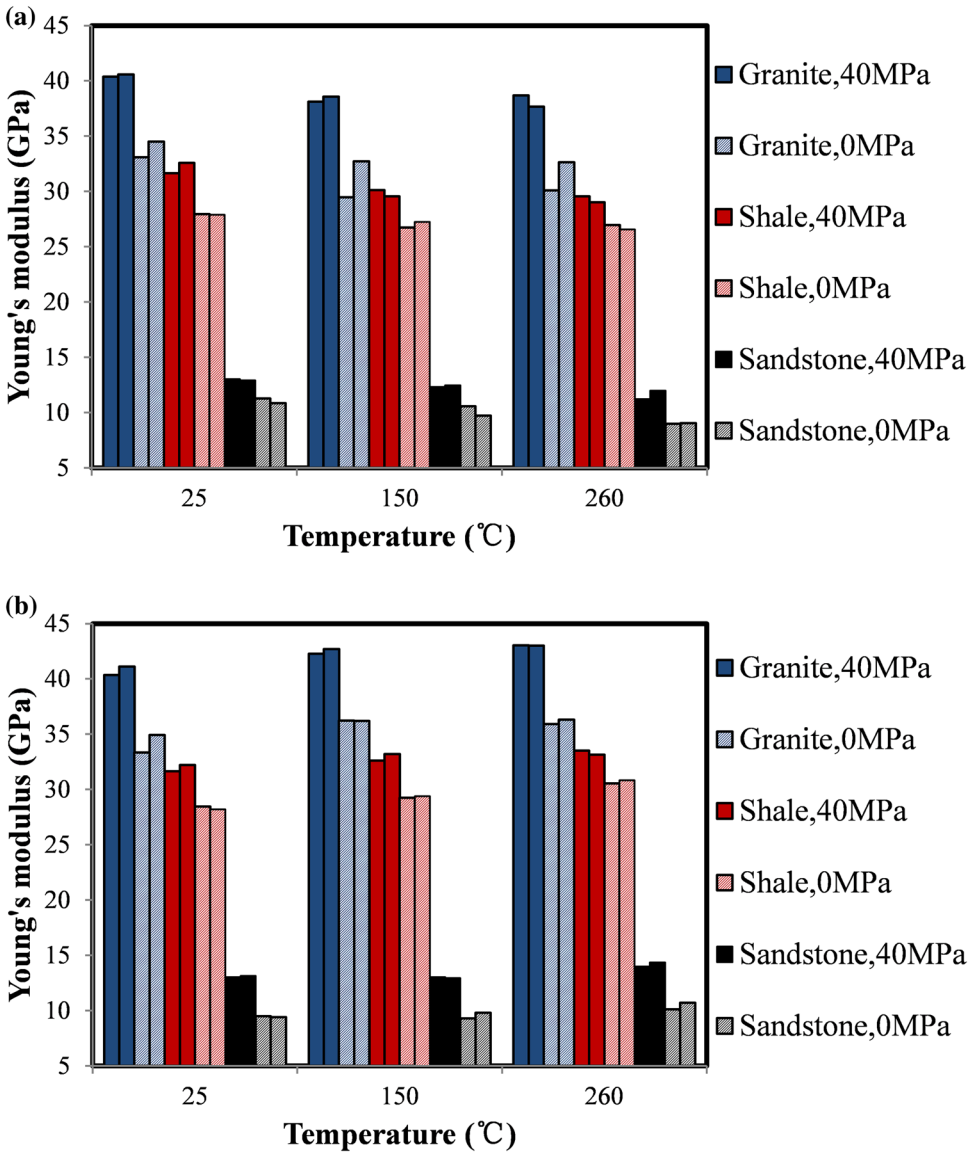

Fig. 10 The comparison in Young's modulus between confined and unconfined conditions. **a** Rocks subjected to LN_2 cooling; **b** rock subjected to air cooling

and LN_2 cooling deteriorates the shale and granite samples significantly, leading to a great reduction in failure stress. The reduction magnitude of the failure stress also grows with increasing temperatures.

In a certain temperature range, heating treatment can increase the rock strength by inducing the plastic expansion of minerals and improving frictions between the mineral particles (Ferrero and Marini 2001; Ranjith et al. 2012). Due to the slow cooling rate, air cooling cannot induce significant thermal shock. Thus, the strength deterioration in the air cooling stage is not sufficient to compensate the strength improvement generated in the heating stage. That explains why strengths of rocks subjected to heating and air cooling treatments are higher than the strengths of intact rocks. In contrast, due to the strong thermal shock effect of LN_2 cooling, the strength deterioration in the cooling process is quite significant and is even more pronounced than the strength improvement induced by heating. Hence, the strengths of rocks reduce significantly after heating and LN_2 cooling treatment.

To evaluate the mechanical deterioration induced by LN_2 thermal shock, strength after heating and air cooling treatment is taken as a benchmark in this section. Similar to the permeability reduction rate, the rate of strength reduction induced by thermal shock $\Delta\sigma_c$ is given as follows:

$$\Delta\sigma_c = \frac{\sigma_{ca} - \sigma_{cl}}{\sigma_{ca}}. \tag{5}$$

Figure 9 shows the $\Delta\sigma_c$ results of the three rocks under different confining conditions. Whether under confined or unconfined condition, the $\Delta\sigma_c$ values of the sandstone are significantly lower than those of the other two rocks. For the

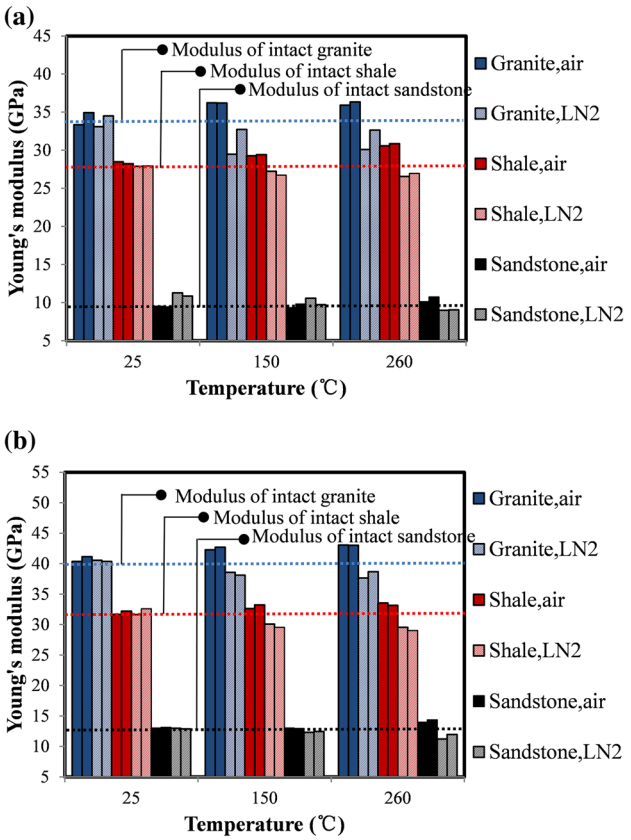

Fig. 11 The comparison in Young's modulus between LN_2 cooling and air cooling. **a** Tested under unconfined condition; **b** tested under the confining pressure of 40 MPa

sandstone at 25 °C and 150 °C, values of the strength reduction rate $\Delta\sigma_c$ are negative, which means that the strengths of sandstone samples are even improved after LN_2 cooling. For shale and granite at 25 °C, the $\Delta\sigma_c$ values are approximately 0%. This fact indicates that the LN_2 thermal shock cannot damage the room-temperature rocks. However, the thermal shock-induced strength reduction rate $\Delta\sigma_c$ shows an increasing trend with temperature. When heating the samples up to 150 °C or 260 °C, LN_2 thermal shock deteriorates the strengths of shale and granite significantly. Based on this phenomenon, we can conclude that higher rock temperatures help strengthen the effect of thermal shock, making the damage of rocks more severe in the cooling process. In addition to the temperature, confining pressure in the test also has a significant influence on mechanical behaviors of rocks subjected to LN_2 thermal shock. According to the results shown in Fig. 9, magnitudes of the strength reduction rate $\Delta\sigma_c$ under confined condition are greatly lower than those under unconfined condition, which is consistent with the permeability results in 3.1. The negative influence of confining pressure is attributed to the densification of rocks under highly confined condition. The densification makes rock samples more difficult to fail in the compression test.

3.2.3 Young's modulus *E*

The Young's modulus is another important parameter in the evaluation of mechanical deterioration; thus we analyzed the influence of thermal loading on the modulus in this section. Figure 10a, b shows the modulus results of rocks subjected to LN_2 cooling and air cooling, respectively. For either cooling way, confining condition has a great impact on the modulus. Among the three rocks, granite has the highest Young's modulus, followed by shale and sandstone. Compared with the modulus tested under unconfined condition, the modulus tested under the confining pressure of 40 MPa is relatively higher. Figure 11a, b illustrates the results of the Young's modulus tested under the unconfined condition and the confined condition, respectively. The Young's modulus is also greatly influenced by cooling ways. Whether for the unconfined condition or the confined condition, Young's modulus of rocks cooled with LN_2 cooling is lower than that cooled in air, and the difference in modulus between two cooling ways becomes greater with increasing rock temperatures, which is consistent with the variation trend of permeability and failure stress again. Therefore, the modulus results can further substantiate that higher rock temperature can strengthen the thermal shock effect and help LN_2 cooling deteriorate the modulus of rocks more significantly.

3.2.4 Failure mode

In this section, we compared and analyzed the failure modes of the three rocks after compression loading. Figure 12a, b shows the failure modes of granite samples cooled in air and cooled in LN_2, respectively. The granite at room temperature shows a tensile splitting failure mode, and it seems that there is a transformation from the tensile splitting failure mode to the shear failure mode as the heating temperature increases gradually. But no significant differences in the failure mode between air cooling and LN_2 quenching are observed. In addition, there are many local fissures near the main failure fracture on granites at 250 °C, which are not noticeable on the granite samples at lower heating temperatures (25 °C and 150 °C). The reason for this phenomenon is that higher temperature strengthens the rock damage and generates more local micro-cracks, which propagate and merge into macro fissures in the compression loading process. Figure 13a, b presents the failure modes of sandstone samples subjected to air cooling and LN_2 quenching, respectively. The primary failure mode of the sandstone is shear failure, and the difference in the failure mode between the two cooling methods is not significant either. As the rock temperature rises, the color of sandstone changes to reddish from beige, and more macro-cracks appear on the rock surfaces after compressive loading. Figure 14a, b shows the failure

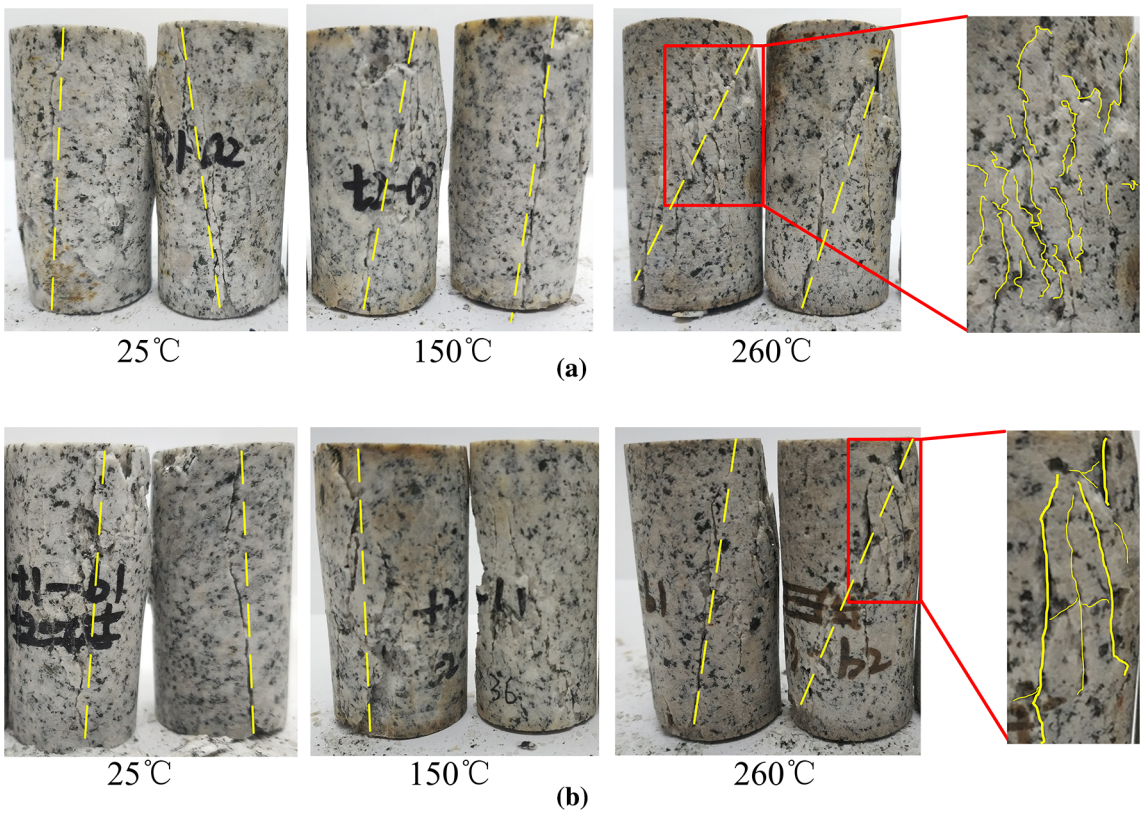

Fig. 12 Failure modes of granites subjected to **a** air cooling and **b** LN_2 cooling

modes of shale samples subjected to air cooling and LN_2 quenching, respectively. It can be found that the shales fail in a tensile splitting mode, and the failure mode does not change with increasing temperatures. The overall integrity of shale, especially for the shale samples subjected to LN_2 thermal shock, is worse than that of the other two rocks after compressive loading. During compressive loading, sheet-like peeling as shown in Fig. 15 occurs in shale. This phenomenon may mainly result from the propagation of the thermally induced micro-cracks along bedding planes during the mechanical tests.

3.3 Micro-structures

Figure 16a–c shows the micro-cracks of granite, shale and sandstone after LN_2 cooling, respectively. According to the SEM images, inter-granular cracks are the primary contributions to the mechanical deterioration and permeability enhancement of rocks, and they mainly appear at the boundaries of quartz. Quartz has significantly greater thermal expansion coefficients than the other minerals; thus thermal loading can lead to larger deformation discrepancy and induce higher local thermal stress at the boundaries of quartz. Due to the larger particle sizes, the inter-granular crack sizes of sandstone and granite are significantly greater than those of shale. Besides the inter-granular cracks, intra-granular cracks can also be generated in rocks after thermal loading, as shown in Fig. 17. These intra-granular cracks are mainly caused by the mineral deformation discrepancy in different crystallographic directions. Since sizes of the intra-granular cracks are significantly smaller than those of the inter-granular cracks, the contribution of the intra-granular cracks to the rock deterioration is relatively limited.

4 Discussion

According to the results of the physical and mechanical properties of the three rocks, granite is the most susceptible to be damaged by LN_2 thermal shock, followed by shale and sandstone. For granite and shale, significant permeability growth and strength drop are caused after LN_2 quenching, and the changing magnitude of these properties increases with temperatures. Unlike the granites and shales, the sandstones are less sensitive to LN_2 thermal shock. The mechanical properties of sandstone samples do not deteriorate a lot after LN_2 cooling, and at lower temperature (like 25 °C) strength of sandstone is even improvrd after LN_2 cooling. To determine the causes of the difference in sensitivity to thermal shock, we analyzed the mineral composition, pore size,

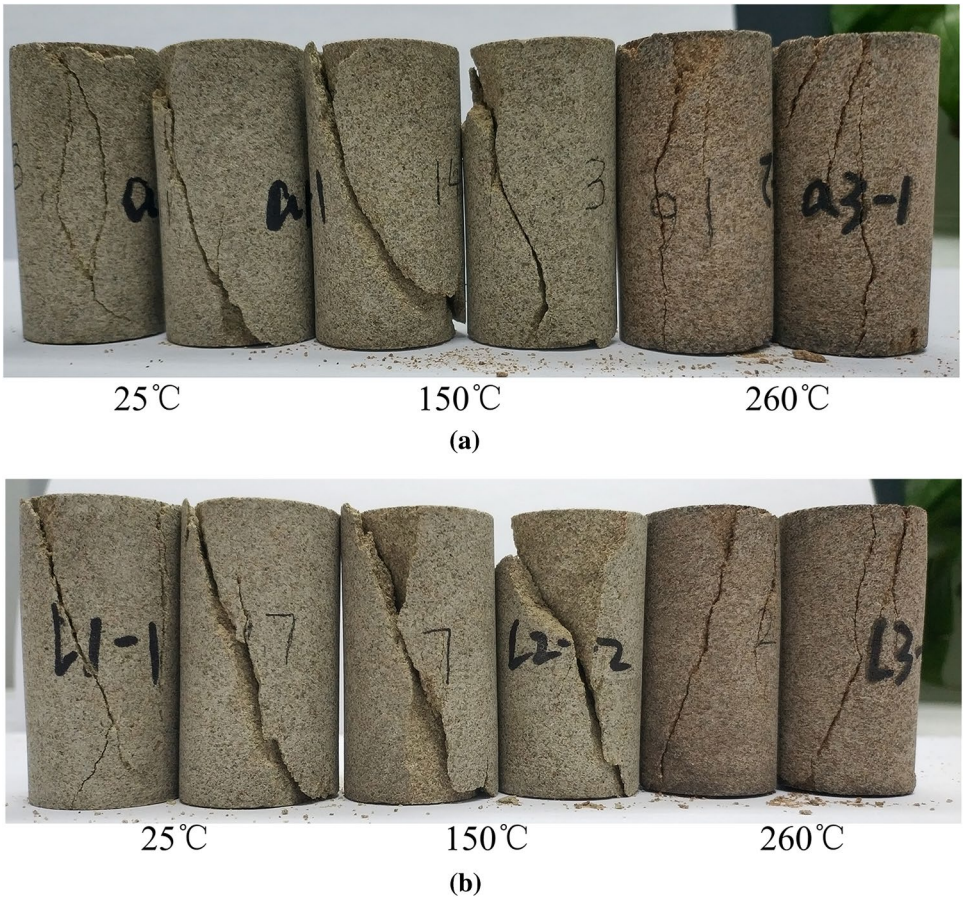

Fig. 13 Failure modes of sandstones subjected to **a** air cooling and **b** LN_2 cooling

diagenesis and cement structure of the three rocks, which are the primary influencing factors of thermal damage.

4.1 Effect of mineral thermal expansion heterogeneity

We tested the mineral composition of the three rocks using XRD. The mineral thermal expansion coefficient is closely related to the rock damage in the thermal loading process. A larger discrepancy in the thermal expansion coefficients between different minerals can induce more severe damage. However, the thermal expansion coefficient data of rock minerals are rarely reported. We only find limited thermophysical property data of minerals and list them in Table 5. According to Table 5, the thermal expansion coefficient of quartz is significantly larger than that of the other minerals, and the thermal expansion coefficients of minerals other than quartz are similar to each other. Hence, the content quartz has a great influence on the heterogeneity of the thermal expansion coefficient, and particular focus is put on the quartz content in this paper.

The XRD results of the three rocks are shown in Fig. 18 and Table 6. Among the three rocks, granite contains the most mineral species, followed by the shale and sandstone. The granite is mainly composed of quartz (28.3%), plagioclase (41.9%) and K-feldspar (15.7%), while the sandstone is mainly composed of quartz (56.9%) and plagioclase (19.1%). The main composition minerals of the shale are quartz (44.1%), dolomite (12.6%), calcite (18.8%) and clay minerals (20.6%). Illite accounts for 95% of the total clay minerals of the shale.

According to the SEM observation shown in Fig. 16a–c, inter-granular cracks between mineral particles are the primary failure modes for rocks in the heating and subsequent cooling process. Hence, the mineral thermal expansion coefficient heterogeneity has a great impact on the sensitivity of rocks to thermal shock. To evaluate the mineral thermal expansion coefficient heterogeneity of the three rocks, the variation coefficient VC was adopted in our analyses. The VC has long been used in the evaluation of reservoir permeability heterogeneity and can also be used to evaluate the heterogeneity of other rock parameters (Ahmed 2006). The VC of the mineral thermal expansion coefficient is calculated by using Eq. 6:

$$\mathrm{VC} = \frac{\sigma}{\beta}. \tag{6}$$

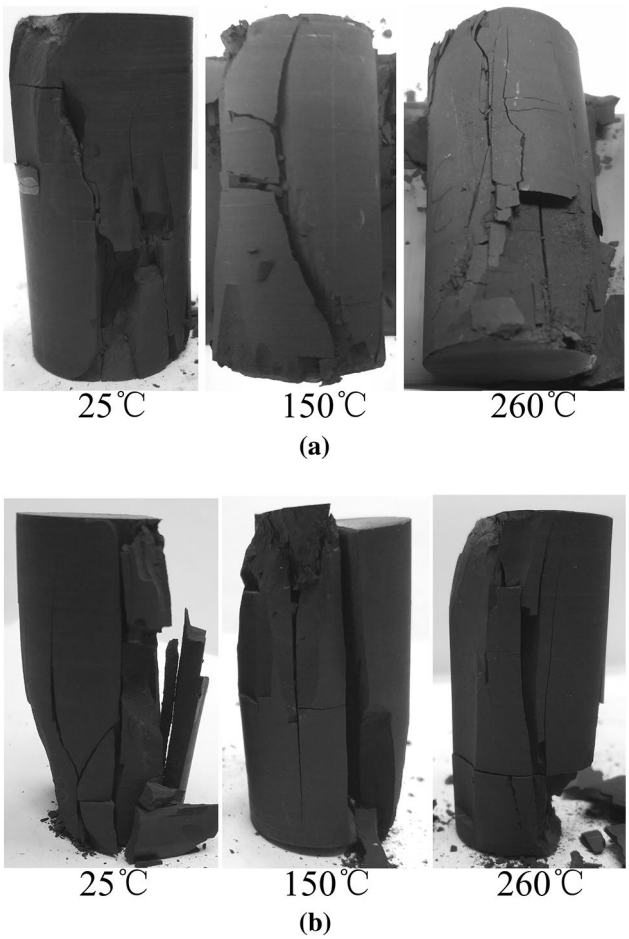

Fig. 14 Failure modes of shale samples subjected to **a** air cooling and **b** LN_2 cooling

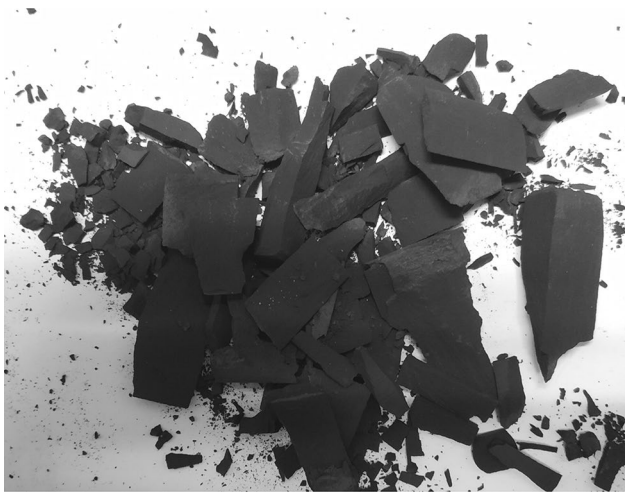

Fig. 15 The peeled sheets of shale after compressive loading

Considering that the thermal expansion coefficients of the minerals other than quartz are similar to each other, we divide the minerals into two groups: (1) the quartz group and (2) the non-quartz group. Since the thermal expansion coefficients of minerals other than quartz are within the range of $5 \sim 8.6 \times 10^{-6}$/℃, as shown in Table 5, we take the median of this range (6.8×10^{-6}/℃) as the average thermal expansion coefficient of the non-quartz group. The thermal expansion coefficient of quartz is assumed to be the average value of the quartz data in Table 5, namely 20.45×10^{-6}/℃. The average thermal expansion coefficient β for a given rock is calculated by Eq. 7:

$$\beta = \beta_q \times \varphi + \beta_{nq} \times (1 - \varphi). \tag{7}$$

Table 7 shows the calculation results of VC. It is obvious that the VC of granite is the highest, while the VC of sandstone is the lowest. This indicates that the heterogeneity of mineral thermal expansion coefficient of sandstone is significantly lower than that of the other two rocks. For rocks with higher mineral thermal expansion heterogeneity, more local failures can be generated in the thermal loading process. This explains why the sandstone is less sensitive to LN_2 thermal shock compared with the other two rocks in our work.

4.2 Effect of the original pore space size

The original pore space size of rock is another important factor that affects thermal damage. The SEM images can be used to evaluate the rock porosity level qualitatively. Figure 19a–c show the micro-structures of the intact granite, shale and sandstone, respectively. For granite and shale, as shown in Fig. 19a, b, the particles are cemented tightly, and the pore sizes are on the order of a few microns. However, for the sandstone (shown in Fig. 19c), the mineral particles are relatively larger. There are many large pore spaces on the order of several hundred microns. The large pore space in the sandstone is able to accommodate the thermal deformation in the thermal loading process, weaken the constraints between the mineral particles and thus help reduce local thermal stresses and the associated thermal damage. In contrast, for the rocks with small pore spaces, such as granite and shale, the thermal stresses between particles are significantly higher than those in sandstone due to the tight constraints. There are no enough spaces to accommodate the deformation in the thermal loading process for such rocks. Therefore, the small original pore space is one of the potential reasons for the significant thermal damage of granite and shale. Additionally, according to previous studies (Zhao et al. 2018), the grain size also significantly influences the thermally induced damage. With increasing grain size, the magnitude of the rock strength reduction induced by thermal

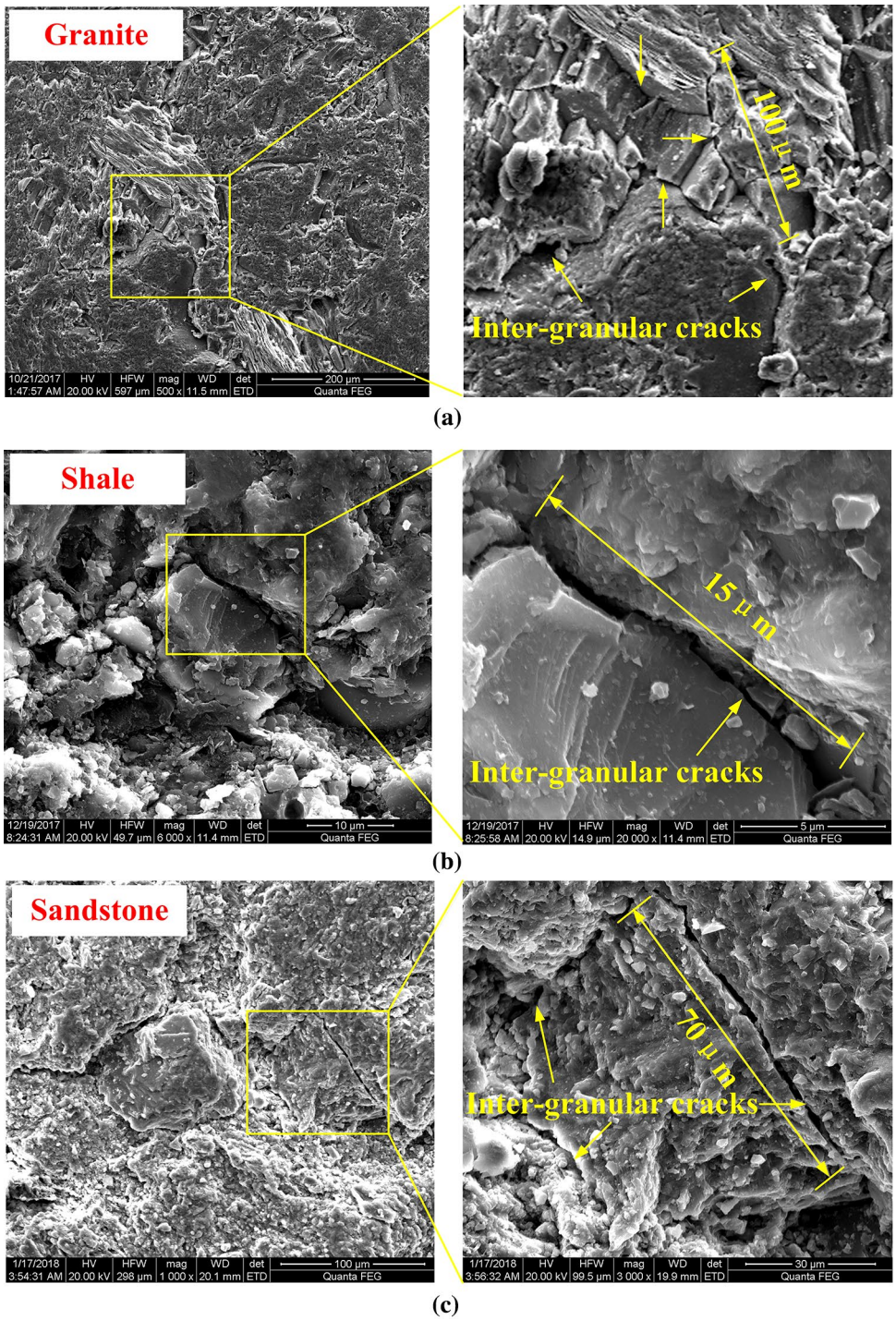

Fig. 16 Micro-cracks of **a** granite, **b** shale and **c** sandstone (260 °C) subjected to LN_2 thermal shock

loading decreases. Nevertheless, the grain size of rocks is closely related to the pore size. Generally, the larger the grain size is, the larger the average pore space. Hence, the effect of the grain size on the thermally induced damage is virtually the same as the pore space effect.

4.3 Effect of diagenesis and cement structure

Diagenesis and the cement structure determine the microstructure and mineral composition of rocks and thus may also have some impact on the sensitivity to thermal shock. Granite, as an igneous rock, is a product of magmatic activity during early diagenesis. After invading into the upper formation, the molten magma is gradually cooled, crystallized and solidified

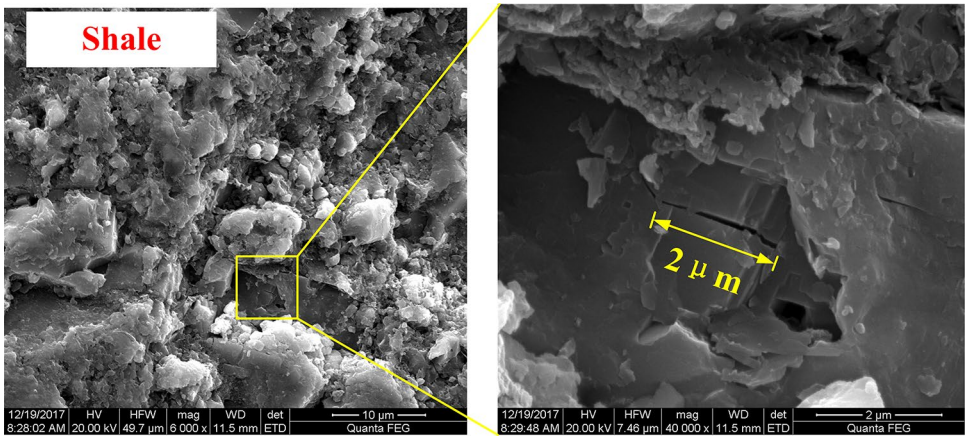

Fig. 17 The intra-granular cracks of shale (260 °C) subjected to LN_2 thermal shock

Table 5 Uniaxial thermal expansion coefficient of minerals (Ahrens 1995; Igarashi et al. 2015; Johnson and Parsons 1944)

Mineral	Uniaxial thermal expansion coefficient ($\times 10^{-6}$/°C)
Quartz	16.6; 24.3
Pyrite	8.6
Microcline	6.0; 5.2
Orthoclase	5.1; 3.2
Anorthite	5.0; 7.5
Albite	7.5; 8.9
Dolomite	7.6
Calcite	6.7

to granite rock. Hence, granite is actually a crystalline rock in which mineral particles are closely arranged and cemented by the growing crystals. The close arrangement can reinforce the mutual restraint between the particles and produce strong thermal stress in the rocks during temperature changes, making the granite less durable to thermal shock. However, sedimentary rock, such as sandstone, is formed by the compaction and cementation of weathered deposits. The formation depth of sandstone is usually significantly lower than that of granite, which makes the arrangement of sandstone grains looser. During diagenesis, sedimentary rocks suffer from a series of effects, including the compaction effect, cementation effect, alteration effect, etc. In the cementation process of sandstone,

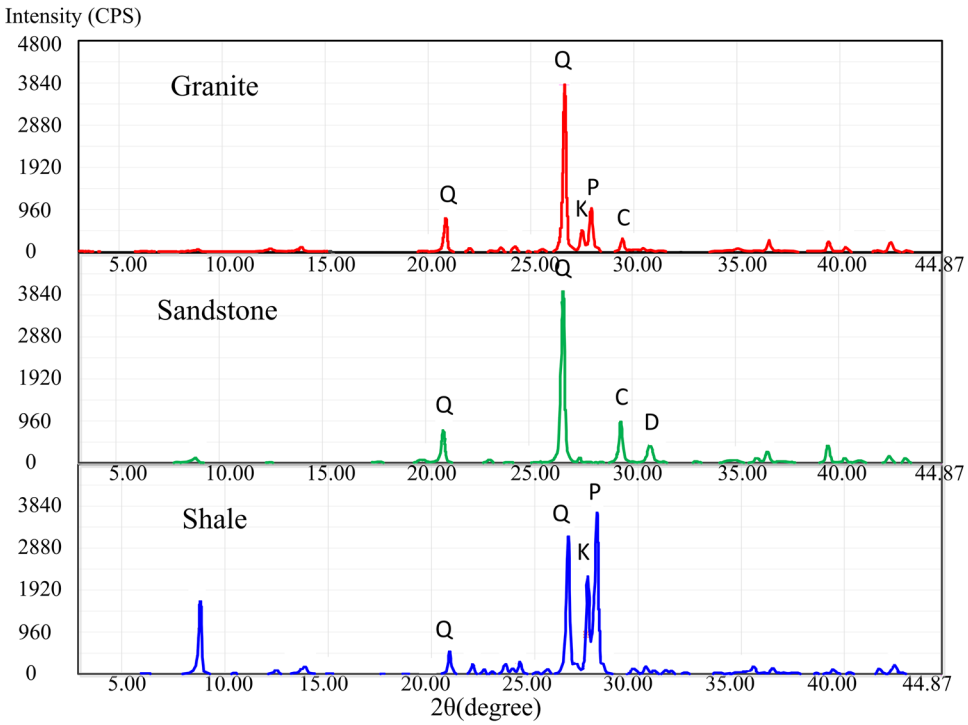

Fig. 18 XRD results of three rocks

Table 6 Mineral compositions of three different rocks

Minerals	Q	K	P	C	D	St	A	Py	Clay minerals
Granite	28.3%	15.7%	41.9%	1.0%	1.9%	0.8%	1.0%	5.8%	3.6%
Shale	44.1%	1.9%	0.7%	18.8%	12.6%	–	–	1.3%	20.6% (95% illite)
Sandstone	56.9%	9.6%	19.1%	6.4%	–	–	–	–	8.0%

Q quartz, *K* K-feldspar, *P* plagioclase, *C* calcite, *D* dolomite, *St* stone salt, *A* amphibole, *Py*pPyroxene

Table 7 VC results of three rocks

Rock species	Quartz content φ	Non-quartz mineral content (1-φ)	Average β	Standard deviation σ	VC
Sandstone	0.569	0.431	14.567	6.794	0.466
Shale	0.440	0.560	12.806	6.810	0.532
Granite	0.280	0.720	10.622	6.160	0.580

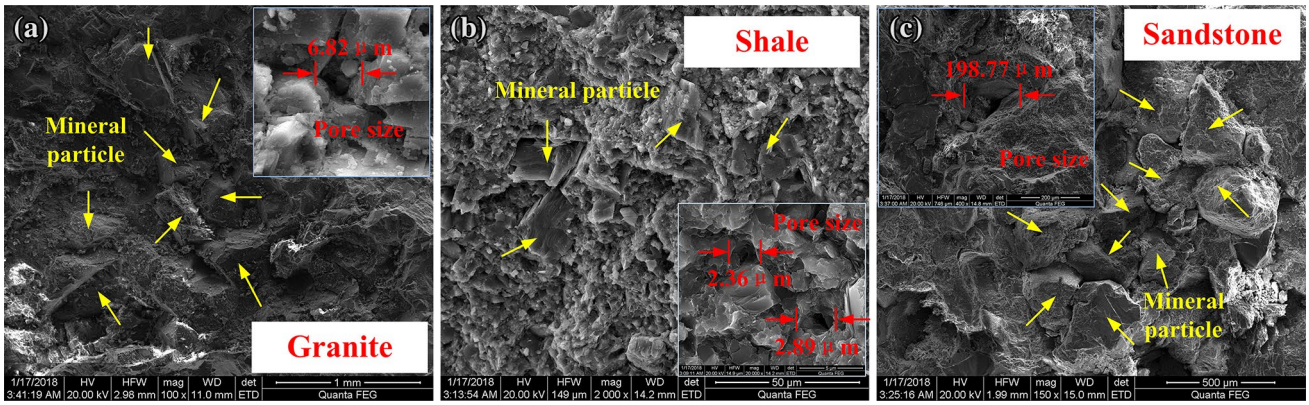

Fig. 19 Micro-structures before thermal loading: **a** granite, **b** shale and **c** sandstone

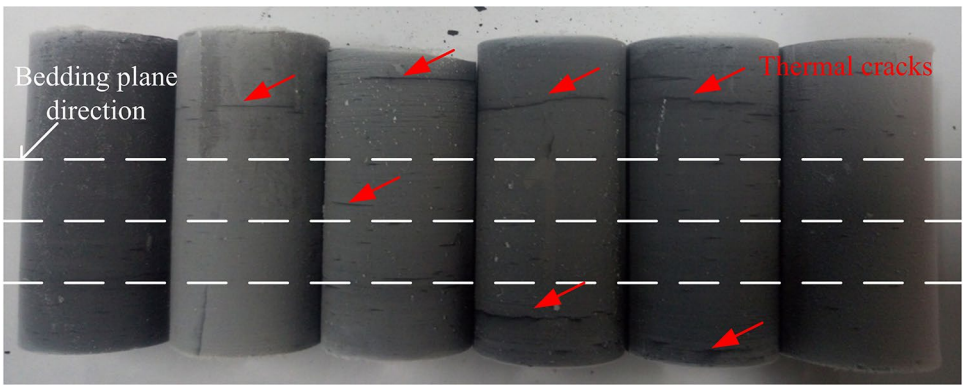

Fig. 20 Cracking pattern of shale subjected to LN_2 thermal shock

some silicate minerals, such as K-feldspar and Na-spar, are dissolved into the cement materials. The mineral dissolution may further enlarge the pore space and reduce the mineral heterogeneity of sandstone and thus make sandstone more resistant to thermal shock than granite. Shale is also a sedimentary rock. However, unlike sandstone, shale is more prone to be damaged by the thermal shock. This may have resulted from the weak cementation at the bedding planes in shale. Shale is formed by compaction, dehydration and recrystallization of clay materials. Many bedding planes form in the compaction stage during diagenesis. Cementation at the bedding plane is relatively weak and can be easily cracked by thermal loading. Figure 20 shows the cracking pattern of shale subjected to LN_2 thermal shock. It is seen that most of the thermal cracks initiate and propagate along the bedding planes. Hence, the bedding planes may make shales less resistant to the thermal shock.

5 Conclusions

In the present paper, we compared and analyzed the damage characteristics of three different high-temperature rocks (sandstone, shale and granite) subjected to LN_2 thermal shock. The main conclusions are summarized as follows:

1. The thermal shock effect of LN_2 shows an excellent performance in improving permeability and deteriorating mechanical properties of rocks. Compared with granite and shale, sandstone is less sensitive to LN_2 thermal shock. The physical and mechanical responses of the sandstone to thermal shock are not as noticeable as those of the other two rocks.
2. Increasing rock temperature can strengthen the LN_2 thermal shock effect significantly, leading to more significant mechanical deteriorations and permeability enhancement.
3. Both inter-granular and intra-granular cracks can be created in rocks during thermal loading. The inter-granular cracks have significantly larger size than the intra-granular cracks do, and thus they are the primary contributions to the damage of rocks subjected LN_2 thermal shock.
4. The sensitivity of rocks to thermal shock mainly depends on microstructure and mineral composition. The low sensitivity of sandstone to LN_2 cooling is attributed to the larger void space and the weaker heterogeneity of mineral thermal expansion. Additionally, bedding planes can facilitate the rock damaged in the LN_2 cooling process.

Acknowledgements This work was supported by the National Science Fund for Distinguished Young Scholars (No. 51725404) and the '111' project of China (No. 110000203920170063).

References

Ahmed T (2006) Reservoir engineering handbook. Gulf Professional Publishing, Oxford

Ahrens TJ (1995) Mineral physics & crystallography: a handbook of physical constants. American Geophysical Union, Washington DC

Alqatahni NB, Cha M, Yao B, Yin X, Kneafsey TJ, Wang L, Miskimins JL (2016, May) Experimental investigation of cryogenic fracturing of rock specimens under true triaxial confining stresses. In: SPE Europec featured at 78th EAGE conference and exhibition. Society of Petroleum Engineers

Breede K, Dzebisashvili K, Liu X, Falcone G (2013) A systematic review of enhanced (or engineered) geothermal systems: past, present and future. Geothermal Energy 1:4

Cai C, Li G, Huang Z, Shen Z, Tian S, Wei J (2014) Experimental study of the effect of liquid nitrogen cooling on rock pore structure.. J Nat Gas Sci Eng 21:507–517

Cai C, Li G, Huang Z, Tian S, Shen Z, Fu X (2015) Experiment of coal damage due to super-cooling with liquid nitrogen. J Nat Gas Sci Eng 22:42–48

Cai C, Huang Z, Li G, Gao F, Wei J, Li R (2016) Feasibility of reservoir fracturing stimulation with liquid nitrogen jet. J Pet Sci Eng 144:59–65

Cha M et al (2014) Cryogenic fracturing for reservoir stimulation—laboratory studies. J Petrol Sci Eng 124:436–450

Ferrero AM, Marini P (2001) Experimental studies on the mechanical behaviour of two thermal cracked marbles. Rock Mech Rock Eng 34:57–66

Ghassemi A (2012) A review of some rock mechanics issues in geothermal reservoir development. Geotech Geol Eng 30:647–664

Hu X, Song X, Li G, Shen Z, Lyu Z, Shi Y, Zheng R (2018a) An analytical model to evaluate the heating conditions for drilling in hard rock using an innovative hydrothermal spallation method. Appl Therm Eng 142:709–716

Hu X, Song X, Liu Y, Li G, Shen Z, Lyu Z (2018b) Aspect ratio of spalls of granite in flame-jet spallation and its effect on the modeling prediction of spallation properties. J Pet Sci Eng 171:1390–1399

Igarashi G, Maruyama I, Nishioka Y, Yoshida H (2015) Influence of mineral composition of siliceous rock on its volume change. Constr Build Mater 94:701–709

Jacobsen RT, Stewart RB, Jahangiri M (1986) Thermodynamic properties of nitrogen from the freezing line to 2000 K at pressures to 1000 MPa. J Phys Chem Ref Data 15:735–909

Johnson B (1978) Thermal cracking of rock subjected to slow, uniform temperature changes. In: Proc. US symp on rock mech 1

Johnson WH, Parsons WH (1944) Thermal expansion of concrete aggregate materials. Government Printing Office, Washington DC

Kim M, Kemeny J (2009) Effect of thermal shock and rapid unloading on mechanical rock properties. Rock Mech Rock Eng 47:2005–2019

Kim K, Kemeny J, Nickerson M (2014) Effect of rapid thermal cooling on mechanical rock properties. Rock Mech Rock Eng 47:2005–2019

Kumari WGP, Ranjith PG, Perera MSA, Chen BK (2017a) Experimental investigation of quenching effect on mechanical, microstructural and flow characteristics of reservoir rocks: Thermal stimulation method for geothermal energy extraction. J Pet Sci Eng 162:419–433

Kumari WGP, Ranjith PG, Perera MSA, Chen BK, Abdulagatov IM (2017b) Temperature-dependent mechanical behaviour of Australian Strathbogie granite with different cooling treatments. Eng Geol 229:31–44

Qin L, Zhai C, Liu S, Xu J (2017a) Mechanical behavior and fracture spatial propagation of coal injected with liquid nitrogen under triaxial stress applied for coalbed methane recovery. Eng Geol 233:1–10

Qin L, Zhai C, Liu S, Xu J, Yu G, Sun Y (2017b) Changes in the petrophysical properties of coal subjected to liquid nitrogen freeze-thaw—a nuclear magnetic resonance investigation. Fuel 194:102–114

Qin L, Zhai C, Liu S, Xu J (2018a) Infrared thermal image and heat transfer characteristics of coal injected with liquid nitrogen under triaxial loading for coalbed methane recovery. Int J Heat Mass Transf 118:1231–1242

Qin L, Zhai C, Liu S, Xu J, Wu S, Dong R (2018b) Fractal dimensions of low rank coal subjected to liquid nitrogen freeze-thaw based on nuclear magnetic resonance applied for coalbed methane recovery. Powder Technol 325:11–20

Ranjith PG, Viete DR, Chen BJ, Perera MSA (2012) Transformation plasticity and the effect of temperature on the mechanical behaviour of Hawkesbury sandstone at atmospheric pressure. Eng Geol 151:120–127

Shao S, Wasantha PLP, Ranjith PG, Chen BK (2014) Effect of cooling rate on the mechanical behavior of heated Strathbogie granite with different grain sizes. Int J Rock Mech Min Sci 70:381–387

Shi Y et al (2018) Numerical investigation on heat extraction performance of a downhole heat exchanger geothermal system. Appl Therm Eng 134:513–526

Tarragó JM, Dorvlo S, Esteve J, Llanes L (2016) Influence of the microstructure on the thermal shock behavior of cemented carbides. Ceram Int 42:12701–12708

Wang L et al (2016a) Waterless fracturing technologies for unconventional reservoirs-opportunities for liquid nitrogen. J Nat Gas Sci Eng 35:160–174

Wang P, Xu J, Liu S, Wang H (2016b) Dynamic mechanical properties and deterioration of red-sandstone subjected to repeated thermal shocks. Eng Geol 212:44–52

Wang P, Xu J, Fang X, Wen M, Zheng G, Wang P (2017) Dynamic splitting tensile behaviors of red-sandstone subjected to repeated thermal shocks: Deterioration and micro-mechanism. Eng Geol 223:1–10

Wenrui H, Jingwei B, Bin H (2013) Trend and progress in global oil and gas exploration. Pet Explor Dev 40:439–443

Wu X et al (2018a) Experiment on coal breaking with cryogenic nitrogen jet. J Petrol Sci Eng 169:405–415

Wu X et al (2018b) Investigation on the damage of high-temperature shale subjected to liquid nitrogen cooling. J Nat Gas Sci Eng 57:284–294

Yang SQ, Xu P, Li YB, Huang YH (2017) Experimental investigation on triaxial mechanical and permeability behavior of sandstone after exposure to different high temperature treatments. Geothermics 69:93–109

Yavuz H, Altindag R, Sarac S, Ugur I, Sengun N (2006) Estimating the index properties of deteriorated carbonate rocks due to freeze–thaw and thermal shock weathering. Int J Rock Mech Min Sci 43:767–775

Zhang S, Huang Z, Huang P, Wu X, Xiong C, Zhang C (2017a) Numerical and experimental analysis of hot dry rock fracturing stimulation with high-pressure abrasive liquid nitrogen jet. J Pet Sci Eng 163:156–165

Zhang S, Huang Z, Li G, Wu X, Peng C, Zhang W (2017b) Numerical analysis of transient conjugate heat transfer and thermal stress distribution in geothermal drilling with high-pressure liquid nitrogen jet. Appl Therm Eng 129:1348–1357

Zhang F, Zhao J, Hu D, Skoczylas F, Shao J (2018) Laboratory investigation on physical and mechanical properties of granite after heating and water-cooling treatment. Rock Mech Rock Eng 51(3):677–694

Zhao Z, Liu Z, Pu H, Li X (2018) Effect of thermal treatment on brazilian tensile strength of granites with different grain size distributions. Rock Mech Rock Eng 51(4):1293–1303

Zhou J, Hu N, Jiang Y, Xian X, Liu Q, Liu G, Tan J (2016) Supercritical carbon dioxide fracturing in shale and the coupled effects on the permeability of fractured shale: an experimental study. J Nat Gas Sci Eng 36:369–377